01 Jan 2014

Investigating the Effect of SiO2-TiO2-CaO-Na 2O-ZnO Bioactive Glass Doped Hydroxyapatite: Characterisation and Structural Evaluation

Chokchai Yatongchai

Anthony W. Wren

Declan J. Curran

Stuart Hampshire

et. al. For a complete list of authors, see https://scholarsmine.mst.edu/che_bioeng_facwork/1135

Investigating the effect of SiO$_2$–TiO$_2$–CaO–Na$_2$O–ZnO bioactive glass doped hydroxyapatite: characterisation and structural evaluation

Chokchai Yatongchai · Anthony W. Wren ·
Declan J. Curran · Stuart Hampshire ·
Mark R. Towler

Abstract The effects of increasing bioactive glass additions, SiO$_2$–TiO$_2$–CaO–Na$_2$O–ZnO up to 25 wt% in increments of 5 wt%, on the physical and mechanical properties of hydroxyapatite (HA) sintered at 900, 1000, 1100 and 1200 °C for 2 h was investigated. Increasing both the glass content and the temperature resulted in increased HA decomposition. This resulted in the formation of a number of bioactive phases. However the presence of the liquidus glass phase did not result in increased densification levels. At 1000 and 1100 °C the additions of 5 wt% glass resulted in a decrease in density which never recovered with increasing glass content. At 1200 °C a cyclic pattern resulted from increasing glass content. There was no direct relationship between strength and density with all samples experiencing no change or a decrease in strength with increasing glass content. Weibull statistics displayed no pattern with increasing glass content.

C. Yatongchai · A. W. Wren
Inamori School of Engineering, Alfred University, Alfred, NY, USA

D. J. Curran (✉) · M. R. Towler
Faculty of Mechanical & Industrial Engineering, Ryerson University, Toronto, ON M5B 2K3, Canada
e-mail: curran@ryerson.ca

S. Hampshire · M. R. Towler
Materials and Surface Science Institute, University of Limerick, Limerick, Ireland

M. R. Towler
Department of Biomedical Engineering, University of Malaya, Kuala Lumpur, Malaysia

1 Introduction

Hydroxyapatite (HA, Ca$_{10}$(PO$_4$)$_6$(OH)$_2$) has excellent bioactivity [1, 2], biocompatibility [3] and osteoconductivity [4–6], which promotes bony in-growth [7]. Stoichiometric-HA is also the most stable calcium orthophosphate, being non-soluble in environments above pH 4.7 [8]. The limiting factor in using HA as an implant is its lack of strength in both tension and shear, confining it to non-load bearing implant situations [9].

There are numerous reports in the literature of employing a second ceramic phase, such as zirconia (ZrO$_2$), to increase the mechanical properties of HA. Synergy is achieved by utilising various processing techniques to form a composite [10–14]. However the increase in mechanical properties is generally obtained at the expense of bioactivity due to solid state interactions between the HA and Zr phases at the elevated temperatures required for Zr densification. This leads to the formation of calcia-stabilised ZrO$_2$ and subsequently, may result in calcium zirconate (CaZrO$_3$). The former reduces the toughening martensitic transformation mechanism of the Zr phase when fully stabilised and the latter results in poor biocompatibility. In addition, the remaining HA that does not undergo solid state reaction can experience increased levels of decomposition [15, 16], adversely affecting biological response [17, 18]. The authors attempted to reduce this by using microwave sintering [19]. Thus the advantage of adding a tougher second phase to increase strength is generally offset by decreased biocompatibility of the composite.

A number of processing techniques have been shown to reduce the level of decomposition of the HA phase. Hot isostatic pressing can reduce the level of decomposition by retaining H$_2$O in the system [20, 21]. Correspondingly, in some instances, spark plasma sintering [22, 23] can prevent decomposition due to its relatively short processing time. The lack of decomposition in these studies may also be

highly dependent on the quality of the starting powders as stoichiometric HA resists decomposition to a greater degree than non-stoichiometric HA. Although the HA phase is retained in these composites and the biocompatibility level kept, the ZrO_2 acts purely as a crack stopper and its relative bioinertness does not impart any biological advantage to the composite.

Strengthening of HA is not limited to using tougher ceramic inclusions as a strengthening phase. The addition of a suitable metal phase can increase the strength of the ceramic due to the ductile nature of the metal, resulting in crack bridging and crack arresting due to direct contact with the metal phase [24–27], although there are instances where this does not occur [28]. Silver (Ag) is one of the more common metals reported in the literature. In addition to a possible increase in strength of the HA matrix, Ag may delay decomposition [26] due to lack of solid state reaction between Ag and HA and sintering in a moist air environment [27]. Silver also adds anti-microbial properties to the composite [28], unlike the ZrO_2 phase which has no biological capabilities. Nevertheless, the high sintering temperatures (>1100 °C) required for densification of a HA–Ag composite can also result in decomposition of the HA phase [24]. Thus it would be ideal to design a HA composite that utilises a second phase that adds strength to the HA, but also maintains or adds to the overall composite bioactivity if degradation of the HA phase were to occur. The addition of a glass phase may provide this scenario. Kokubo et al. [29] developed glass–ceramics containing crystalline apatite and wollastonite ($CaO \cdot SiO_2$), termed A–W, in a glass matrix of $MgO–P_2O_5–CaF_2$ resulting in materials with greater compressive strengths than glass [30, 31], higher strength than sintered HA [32–35] and, in some cases, HA–metal composites [24, 26].

Thus it may be possible to tailor a composite with a glass phase that may react with a decomposing HA, producing secondary crystalline or vitreous phases that are conducive to increased bioactivity and strength of the overall composite. This current work seeks to follow this postulation. The glass phase used is based on a bioactive glass previously reported by the authors [36–39] and consists of CaO, TiO_2, Na_2O, ZnO and SiO_2. Although the authors have reported on HA composites previously [19, 40, 41], this is the first study to combine these two different streams of research in an attempt to increase the applicability of HA for load bearing applications.

2 Experimental methods

2.1 Material processing

2.1.1 Hydroxyapatite (HA) synthesis

Pure HA powder was produced at a synthesis temperature of 25 °C by a simple precipitation method similar to that reported by Jarcho et al. [16]. 78.72 g (0.3335 mol) of calcium nitrate hydrate ($Ca(NO_3)_2 \cdot 4H_2O$) in 600 ml of water was made basic by the addition of 10 ml of ammonium hydroxide (NH_4OH). 26.41 g (0.2000 mol) of di-ammonium hydrogen orthophosphate (($NH_4)_2HPO_4$) was made basic in 1066 ml of water by the addition of 25 ml of NH_4OH. The $Ca(NO_3)_2 \cdot 4H_2O$ and $(NH_4)_2HPO_4$ solutions were stirred vigorously before synthesis to ensure the reagents were completely dissolved. Both solutions were brought to the desired synthesis temperature and, under continued vigorous stirring, the $(NH_4)_2HPO_4$ solution was added drop-wise from a glass funnel into the $Ca(NO_3)_2 \cdot 4H_2O$ solution over a 60 min interval. Throughout the synthesis the pH was kept above 10.0 by the addition of NH_4OH at constant intervals to avoid shock to the system. Once drop-wise addition was completed, the solution was kept at the synthesis temperature for 1 h under the same temperature and vigorous stirring conditions. If the pH had not stabilised after 1 h, stirring was continued until it had done so to ensure complete reaction. The sample was then left to stand for 24 h at room temperature. The supernatant was removed and replaced with fresh distilled water, re-stirred for 1 h and left to stand again for 24 h. This procedure was undertaken three times to remove any unwanted residue from the precipitate. The supernatant was removed a final time and replaced with distilled water and spun for 15 min. The suspension was then filtered under vacuum, using a Buchner filter and distilled water until the ammonia was removed. The filter cake was then removed from the filter and placed into a beaker and dried in a fan assisted oven at 85 °C for 20 h.

2.1.2 Bioactive glass synthesis

The glass, with formulation $0.05CaO–0.12TiO_2–0.17Na_2O–0.28ZnO–0.38SiO_2$, was prepared by mixing appropriate amounts of analytical grade reagents (Sigma-Aldrich, Dublin, Ireland) in a ball mill for 1 h. The mix was then oven dried (100 °C, 1 h). The composition was subsequently melted at 1450 °C for 1 h in a platinum crucible and shock quenched into water. The resulting frit was dried, ground and sieved to retrieve a glass powder with a maximum particle size of 45 μm.

2.1.3 Sample preparation

Green bodies were obtained by mixing the HA powder with incremental glass additions of 5–50 wt%. The mixtures were wet mixed in a ball mill for 3 h with methanol as a suspending medium, subsequently oven dried (75 °C, 24 h) and sieved to a particle size <75 μm in order to obtain a homogeneous powder. The dried powders were uniaxially pressed into pellets using a 15 mm Ø stainless steel die at 200 MPa.

2.2 Material characterisation

2.2.1 Particle size analysis (DTA)

Particle size and specific surface area of the HA powders were determined using a Beckman-Coulter Multisizer 4 (Beckman-coulter, Brea, CA). 1 mg of a dried HA powder was suspended in 100 ml of sodium chloride solution (as an electrolyte solution), and then stirred for 3 min with high speed spinning. After that, the suspension was drawn through a 100 μm aperture tube equipped in the Multisizer 4. Each particle passing through the aperture displaces its own volume of conducting liquid, momentarily increasing the impedance of the aperture. This change in impedance is detected and converted into a voltage pulse large enough to measure accurately.

2.2.2 Density of glass

The powder density of the glass (≈ 4 μm) was measured using helium pycnometry (Micromeritics, AccuPyc 1330, Micromeritics Instrument, USA) with a set pressure of 130 kPa. The sample holder was filled up to 2/3 of the total volume and accurately weighed. The equipment was set to automatically measure the density of the samples five times.

2.2.3 Differential thermal analysis (DTA)

DTA was used to determine the glass transition (T_g) and crystallization temperatures (T_c) of the glass. A TA SDT 2960 instrument (TA Instruments, USA) with a bifilar-wound furnace was used to heat 16 mg (≈ 4 μm) of crushed glass under air flow of 100 mL/min at heating rate of 10 °C/min. The same weight of calcined Al_2O_3 was used as a reference.

2.2.4 Powder X-ray diffraction (XRD)

Following uniaxial compaction, powder compacts were placed in an X-ray Diffractometer (D2 Phaser, Bruker AXS, Germany) and scanned covering a 2θ range from 10° to 70°, with a step size of 0.02° and a step time of 1 s. The XRD patterns were then matched to patterns in the JCPDS and ICSD database, using the X'Pert software. Visual

analysis of the obtained spectra was carried out in Origin Pro 8 (OriginLab Corporation, Massachusetts, USA).

2.2.5 Scanning electron microscopy (SEM)

An FEI Quanta 200F SEM was used to analyse the microstructure of the composite after polishing to 1 μm finish with alumina powder and cleaning in ultrasonic water for 10 min at room temperature.

2.3 Composite evaluation

2.3.1 Sintering

Sintering was performed in a Lindberg/Blue M model furnace (Lindberg/Blue M, Asheville, NC USA) with a UP550 controller as standard. Samples were prepared for sintering by pressing powder in a 15 mm ø stainless steel die. The discs were sintered at a heating rate of 5 °C/min to a maximum temperature of either 900, 1000, 1100 or 1200 °C, with a hold time of 2 h. Following this, samples were allowed to furnace cool.

2.3.2 Density

The bulk density (ρ_b), Eq. 1, was calculated using the Archimedes buoyancy method. This method involved obtaining the sample dry weight in air after the sample was place in a drying oven for 24 h, giving the value W_{air}. The sample was then placed in water and put under vacuum for 1 h, to replace the air in the open pores with water; the sample was then weighed by submerging in water using a hydrostatic balance, giving W_{submer}. The sample was then removed and the excess fluid removed from the surface with a damp sponge before weighing in air to give W_{damp}.

Equation 1: The bulk density of the HA–glass composite (g/cm³). ρ_{fl} is the density of water at 20 °C (0.99823 g/cm³)

$$\rho_b = \frac{W_{air}}{W_{damp} - W_{submer}} \cdot \rho fl \tag{1}$$

The relative bulk density was determined using the following equation:

Equation 2: Percentage relative bulk density of the HA glass composite (%)

$$\rho_{RD} = \frac{\rho_b}{(T.D.P_1 \times wt\,P_1) + (T.D.P_2 \times wt\,P_2) + \cdots (T.D.P_n \times wt\,P_n)} \times 100 \tag{2}$$

Fig. 1 Biaxial flexural testing jig

Where, ρ_{RD} is the relative bulk density; $T.D.P_1$ is the theoretical density of the phase P_1; wt% P_1 is the percentage of that phase detected using quantitative XRD; P_2 signifies the possible second formed phase and P_n signifies any subsequent phases formed in the composite with the addition of the glass phase or HA decomposition.

2.3.3 Biaxial flexural strength (BFS)

BFS was determined using a method similar to that of Williams et al. [42] using three support bearings on the test jig, Fig. 1.

The test jig was fixed to an Instron Universal Testing Machine (Instron 5566, Instron, USA) using a load cell of 5 kN at a crosshead speed of 1 mm/min. Sample thickness was measured at the point of fracture using a digital Vernier calliper. The BFS was calculated according to Williams et al. [42] using Eq. 3. The median BFS was then taken for each sample set at the same temperature and glass content.

Equation 3: Biaxial flexural strength (BFS) of the samples (MPa)

$$BFS(MPa) = \frac{Load(N)}{t^2}\left[(1+\upsilon) \times \left(0.485 \times \ln\left(\frac{a}{t}\right) + 0.52\right) + 0.48\right] \quad (3)$$

where υ is the Poisson's ratio (taken as 0.28), a is the radius of the support diameter (mm), taken as 3.825333 mm, t is the thickness of specimen (mm)

Table 1 Particle size analysis of glass and HA powder

	D_{10} (μm)	D_{50} (μm)	D_{90} (μm)
Glass	2.542	3.863	7.610
HA	2.446	3.519	7.322

2.3.4 Weibull statistics

The Weibull modulus, m, was calculated using the two parameter Weibull probability function, Eq (4), a logarithmic plot of survival probability, Ps, and failure strength, σ.

Equation 4: Weibull probability function

$$P_s = 1 - P_f = \exp\left[-\left(\frac{\sigma}{\sigma_0}\right)^m\right] \quad (4)$$

After measuring the BFS of samples, the values were rank ordered from the weakest to strongest. Based on the ranking of the strength, i, each strength was assigned a failure probability by [43]:

Equation 5: Probability of failure.

$$P_f = \frac{i - 0.5}{n} \quad (5)$$

where n is the total number of specimens.

Plotting lnln[1/(1-Pf)] versus ln σ results in a straight line of slope m.

3 Results

3.1 Material characterisation

The particle size of the glass and HA are similar with the largest variation between the glass phase and the HA phase occurring in the d_{50} values. The density of the glass phase was calculated as 3.15 g/cm³, which is almost identical to the theoretical density of HA of 3.16 g/cm³. Table 1 contains the particle sizes of both the HA and glass powders.

Differential thermal analysis (DTA) of the glass is presented in Fig. 2 and shows the initial endothermic event of the glass transition, the exothermic reaction peaks associated with the formation of crystalline phases and a final endothermic trough corresponding to melting. The endothermic trough of the glass transition temperature (T_g) occurs at 541 °C while the glass displays a large crystallisation peak (T_c) at 620 °C. Two other exothermic peaks occur at 684 and 790 °C, indicating that further crystallisation may be occurring. A final endothermic reaction trough indicates that the liquidus temperature occurs at ~890 °C.

X-ray Diffraction (XRD) is presented in Fig. 3 and was conducted within the temperature range of the DTA traces. XRD was used to identify the phases formed during these exothermic reactions.

Heat-treatment of the glass was carried out for 2 h at 560 °C, i.e. just above Tg, followed by 2 h at 620, 690 and 790 °C. The as-synthesised glass trace and that for the glass heat-treated at 560 °C show only amorphous humps and no crystallinity; hence the material is still in an amorphous glass state. After heat-treatment at 620, 690 and 790 °C for
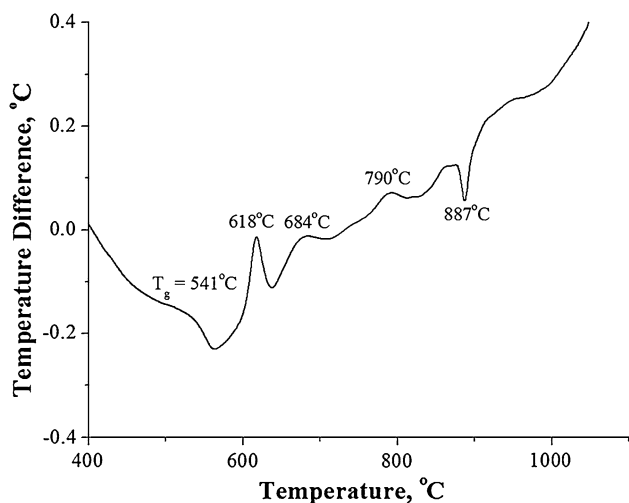
2 h, the XRD suggests consecutive transformation of the parent glass into crystalline phases. The diffraction pattern obtained at 620 °C has been identified as sodium zinc orthosilicate ($Na_2Zn_3(SiO_4)_2$). A further temperature increase to 690 °C defined new phases of hardystonite ($Ca_2ZnSi_2O_7$), zinc metasilicate ($ZnSiO_3$) and zinc oxide (ZnO). After heat-treatment at 790 °C, $Na_2Zn_3(SiO_4)_2$, $ZnSiO_3$, and ZnO, and peaks of calcium titanate ($CaTiO_3$) are observed. Figures 4, 5, 6 and 7 give the XRD phase analysis for the HA and HA/glass composites sintered with a hold time of 2 h at 900, 1000, 1100 or 1200 °C, respectively. It is clear that pure HA is stable up to 1100 °C with only a slight degradation to α-TCP at 1200 °C.

The relative densities at the different temperatures are highly dependent on the reactions between the apatite and glass phase, the resultant phases that are formed and their theoretical densities.

3.2 HA–glass composites sintered at 900 °C

With the incorporation of 5 % glass in HA sintered at 900 °C, the HA undergoes decomposition as β-TCP evolves, implying glass incorporation leads to the destabilisation of the HA by formation of a small volume of liquid (above 887 °C). Upon increasing the glass content to 10 %, reactions exacerbate between the glass/liquid and HA. The β-TCP content increases to similar levels to those of the HA. Hardystonite ($Ca_2ZnSi_2O_7$) also forms part of the phase assemblage. On incorporation of 15 % glass, no

Fig. 2 DTA trace obtained from the powdered glass

Fig. 3 X-ray diffraction patterns for CaO–ZnO–SiO$_2$–TiO$_2$–Na$_2$O glass as-synthesised and heat-treated for 2 h at 560 °C followed by 2 h at 620, 690 and 790 °C
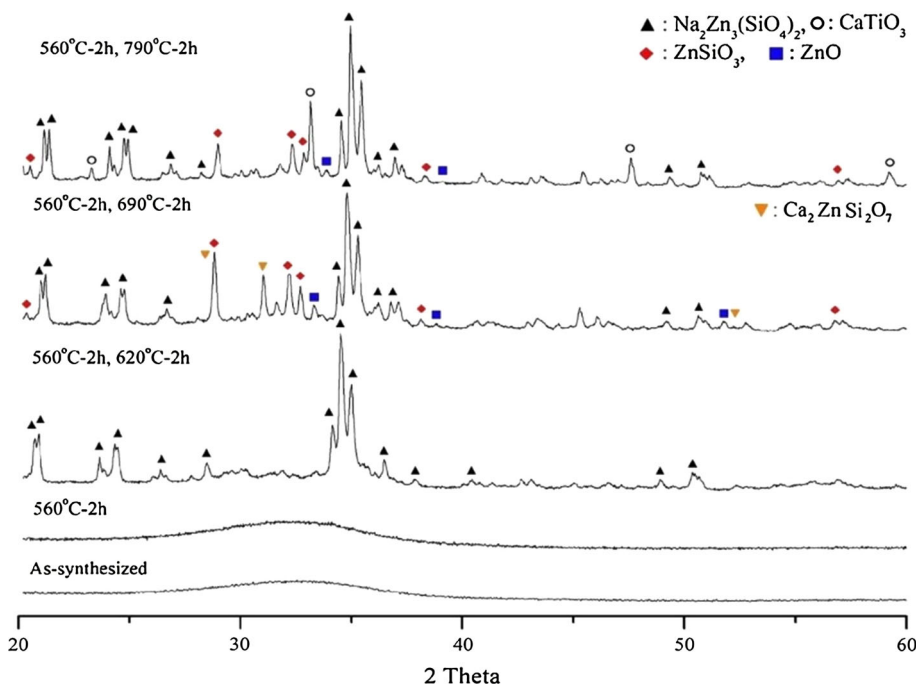
Fig. 4 X-ray diffraction patterns for CaO–ZnO–SiO$_2$–TiO$_2$–Na$_2$O glass as-synthesised and heat-treated for 2 h at 900 °C
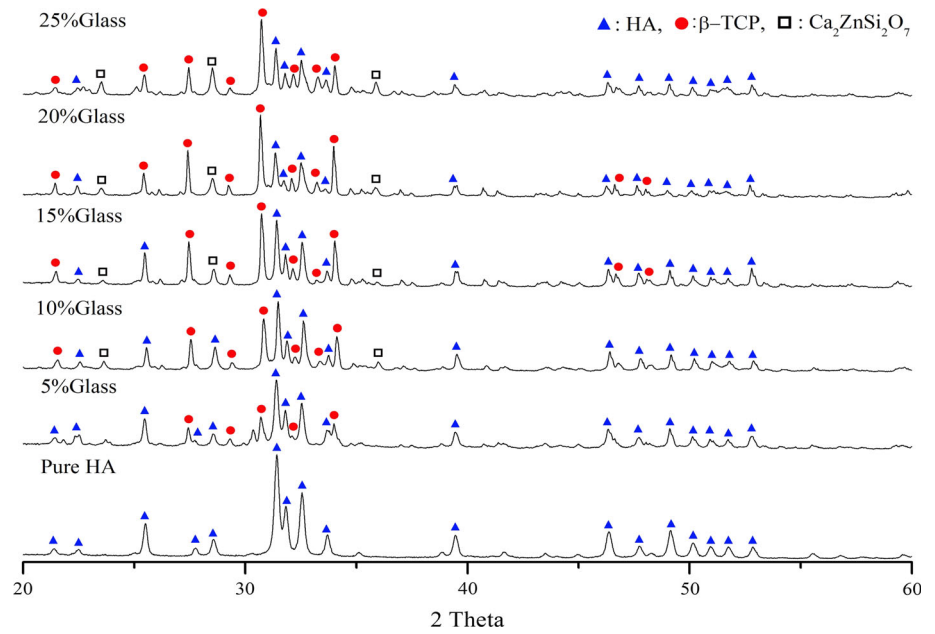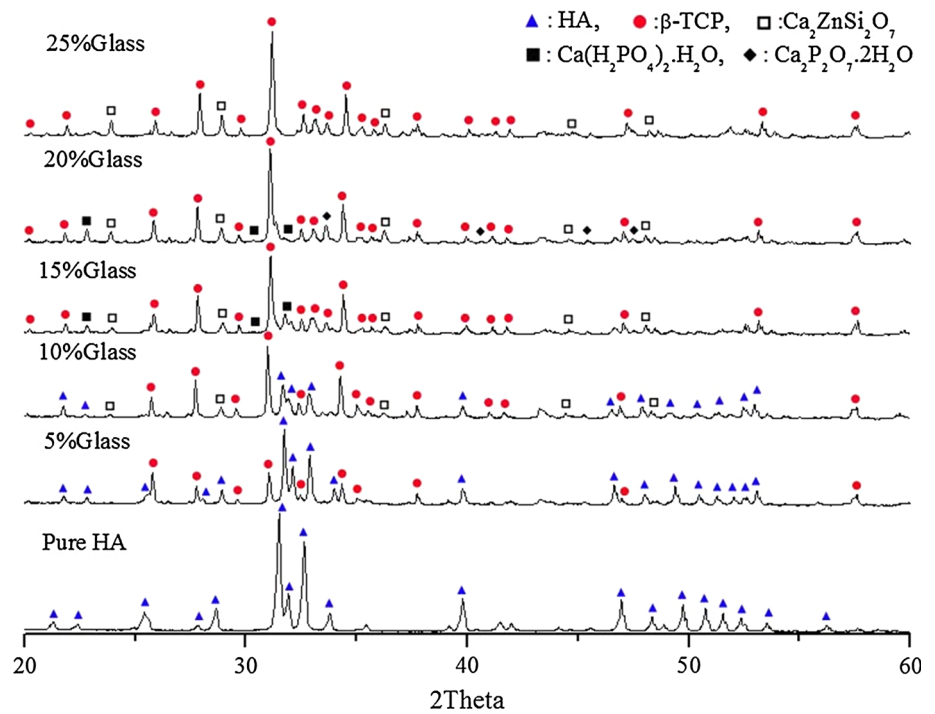

Fig. 5 X-ray diffraction patterns for CaO–ZnO–SiO$_2$–TiO$_2$–Na$_2$O glass as-synthesised and heat-treated for 2 h at 1000 °C

additional phases are formed compared to the samples containing 10 % glass; however, the relative amounts of phases change as the HA decomposes to form β-TCP, which continues up to 25 % glass additions. The level of hardystonite also increases with increasing glass content.

Considering densification during sintering, the samples sintered at 900 °C experience a slight increase in bulk density from 1.67 to 1.87 g/cm^3 (Fig. 8), with a statistical difference of 0.1203 g/cm^3, from 0 to 25 wt% glass content and the samples remain quite porous, displaying a slight increase in relative density of approximately 5 % over the range of added glass content up to 25 wt%. This sintering temperature is only 13 °C higher than the melting temperature of the glass and therefore the liquid phase present would have a high viscosity which would be expected to decrease as sintering temperature increases.

Fig. 6 X-ray diffraction patterns for CaO–ZnO–SiO$_2$–TiO$_2$–Na$_2$O glass as-synthesised and heat-treated for 2 h at 1100 °C
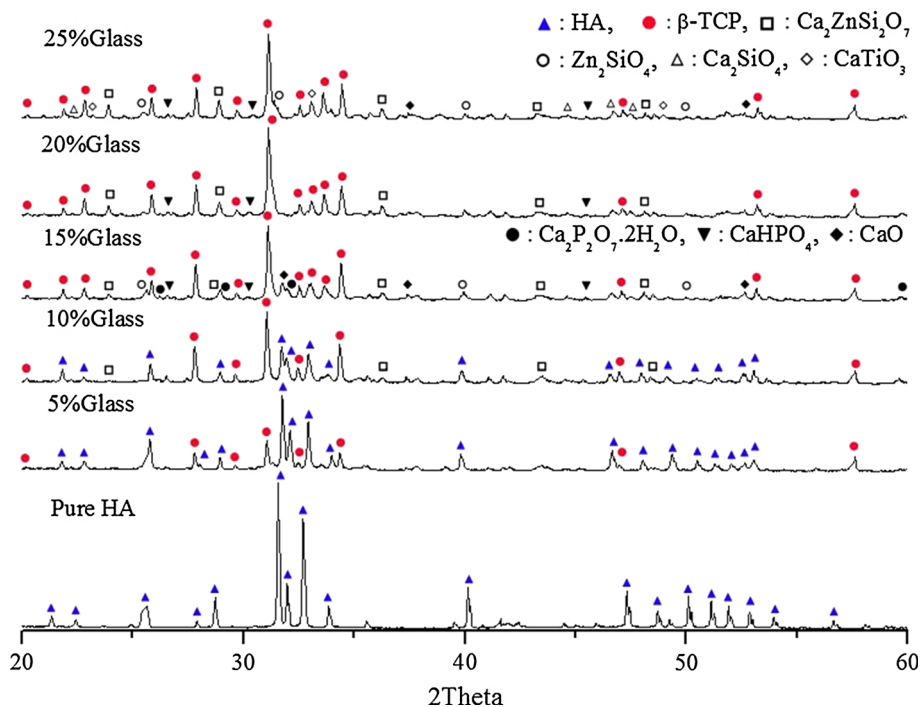

Fig. 7 X-ray diffraction patterns for CaO–ZnO–SiO$_2$–TiO$_2$–Na$_2$O glass as-synthesised and heat-treated for 2 h at 1200 °C
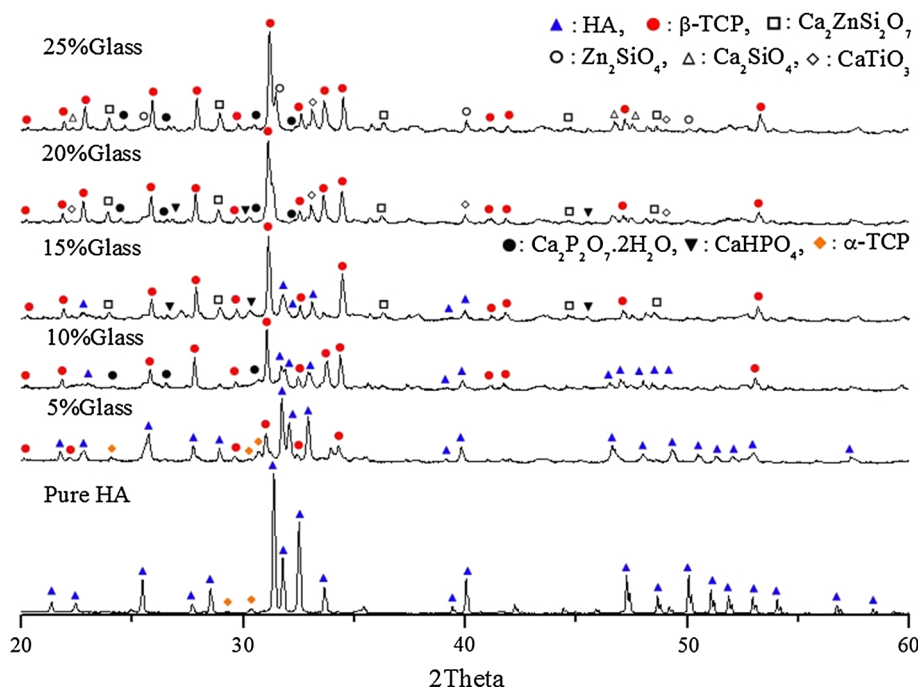
Figure 9 shows SEM images of the HA/glass composites sintered at 900 °C. The samples undergo low levels of sintering as discussed above. This is shown by the relatively large pores and boundary lines seen in Fig. 9a. Increasing the glass content appears to increase the level of porosity in areas where the glass/liquid phase has collected. Figure 9e, f show areas where the liquid phase has coalesced and cools to give a residual glass that can be seen as the large areas of lighter grey material separated from the porous region.

3.3 HA–glass composites sintered at 1000 °C

Increasing the sintering temperature to 1000 °C also results in increased decomposition of the HA phase with increasing glass content. At 15 % glass content the HA

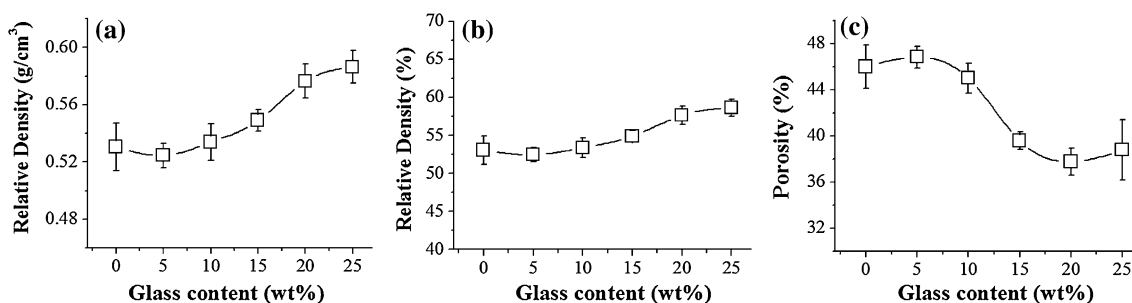**Fig. 8** **a** Bulk density, **b** relative density **c** porosity of HA/glass composites sintered at 900 °C for 2 h
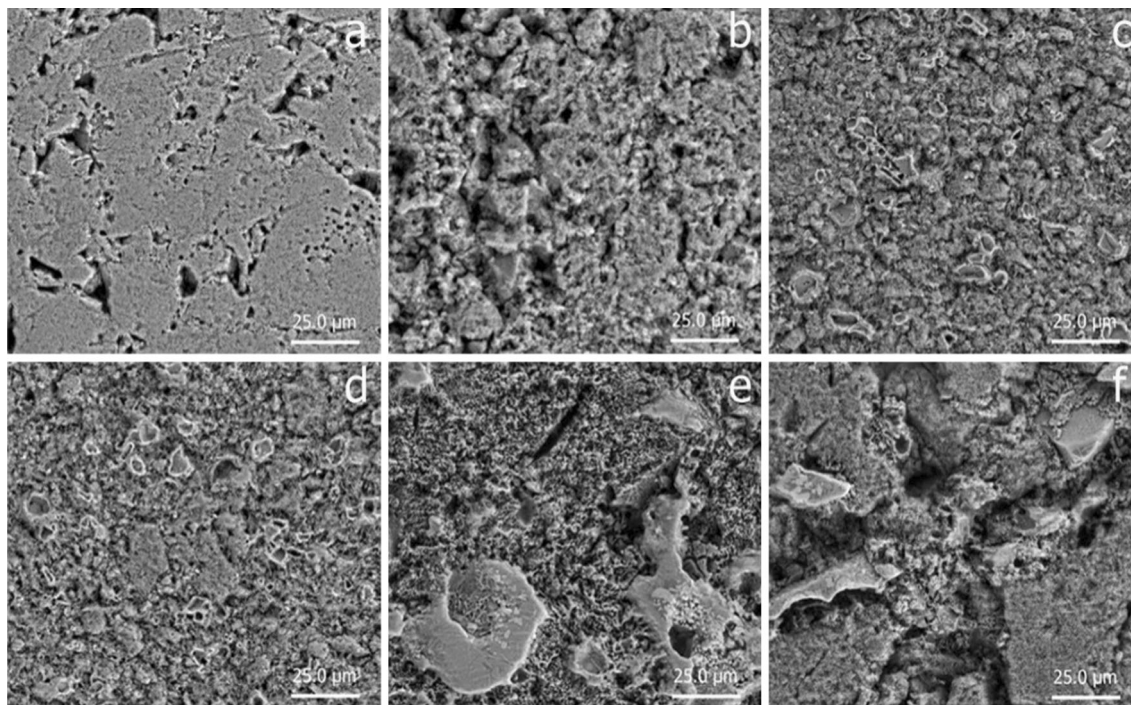

Fig. 9 SEM micrographs for HA/glass composites sintered at 900 °C for 2 h: **a** pure HA, **b** HA/5 % glass, **c** HA/10 % glass, **d** HA/15 % glass, **e** HA/20 % glass and **f** HA/25 % glass

phase has completely decomposed leaving β-TCP as the dominant calcium phosphate phase. In a similar way to HA/glass composites sintered at 900 °C, hardystonite forms at the 10 wt% glass level and increases with up to 25 wt% glass content. Monocalcium phosphate monohydrate ($Ca(H_2PO_4)_2 \cdot H_2O$) forms in the samples containing 15 and 20 wt% glass, while calcium pyrophosphate dihydrate ($Ca_2P_2O_7 \cdot 2H_2O$) forms in the samples containing 20 wt% glass; however, the amounts of these phases are relatively small and are not detected in the composites containing 25 wt% glass.

The pure HA samples sintered at 1000 °C show a relative density of ~ 88 % after which there is a decrease in bulk density, from 2.81 to 1.86 g/cm^3 with the addition of 5 wt% glass (Fig. 10); the relative density decreases

to ~ 60 % and the amount of HA decreases to ~ 65 %. Bulk density remains low with increasing glass content up to 25 wt% display and these samples display no statistical difference in terms of density compared to the samples containing 5 wt% glass. The relative density is relatively unchanged up to 15 % glass content at which point all the HA has reacted to form β-TCP and $Ca_2ZnSi_2O_7$ with other minor phases. The 20 wt% glass samples display a statistically increased relative density of 65 %; however, increasing the glass content up to 25 wt% reduces the relative density again, and is not statistically different from the samples containing 5, 10 and 15 wt% glass sintered at 1000 °C. Thus it appears that as HA reacts with the glass, there is a propensity to form pores, possibly as a result of gasses evolved during the reactions.
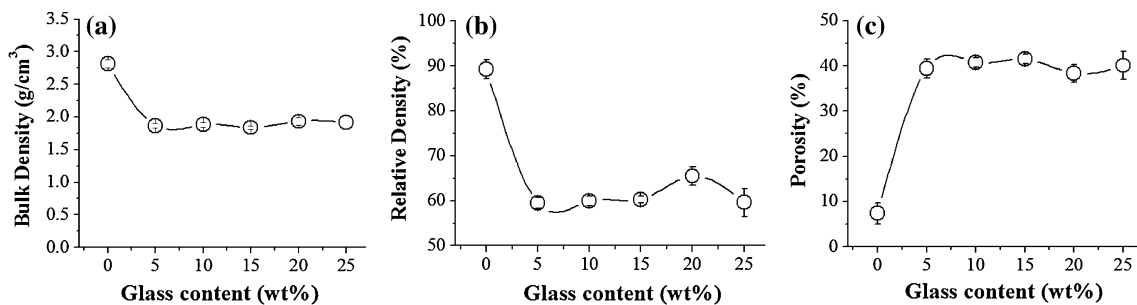
Fig. 10 **a** Bulk density, **b** relative density **c** porosity of HA/glass composites sintered at 1000 °C for 2 h
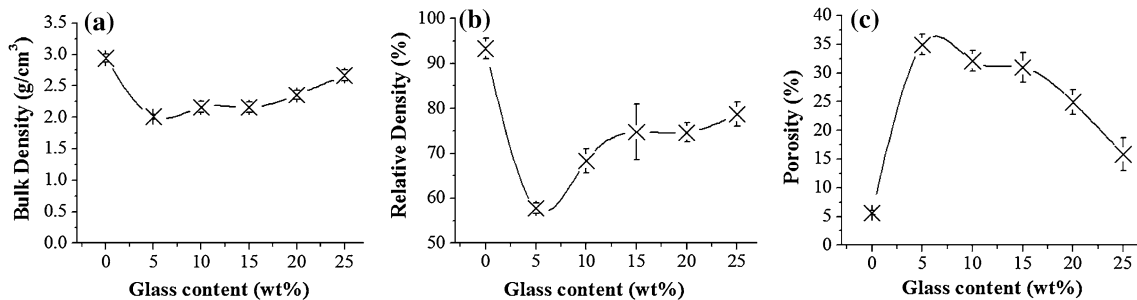

Fig. 11 **a** Bulk density, **b** relative density **c** porosity of HA/glass composites sintered at 1100 °C for 2 h

3.4 HA–glass composites sintered at 1100 °C

At 1100 °C changes in HA and β-TCP follow a similar trend to those in the composites sintered at 1000 °C, with increasing glass content resulting in decreasing HA and increasing β-TCP. Hardystonite forms in composites with 10 wt% glass and increases with up to 25 wt% glass content. Willemite (Zn_2SiO_4) also forms at 1100 °C with 15 wt% glass content. Willemite was not detected in the samples with 20 wt% glass and this may be explained by the higher level of Hardystonite which would be the major phase containing Zn. $Ca_2P_2O_7 \cdot 2H_2O$ also forms in these samples; however, it was only detected in the samples containing 15 wt% glass and at very low levels. Calcium hydrogen phosphate ($CaHPO_4$) forms in the samples containing 15 wt% glass and remains relatively constant with up to 25 wt% glass. Calcium oxide (CaO) forms in relatively small amounts and appears in the samples with 15 and 25 wt% glass. Calcium silicate (Ca_2SiO_4) forms in a relatively small amount in the samples with 25 wt% glass while calcium titanate ($CaTiO_3$) also forms.

The pure HA samples sintered at 1100 °C compact to a higher relative density of ~ 94 % but then there is a substantial decrease to ~ 58 % with addition of 5 % glass as β-TCP forms. Bulk density decreases from 2.94 g/cm^3 for pure HA to 2.01 g/cm^3 for HA containing 5 wt% glass (Fig. 11). Increasing glass content does result in an overall increase, with the final density of the samples containing

25 wt% glass exhibiting a density of 2.67 g/cm^3. This is a statistical difference of 0.53 g/cm^3 compared to the samples containing 5 wt% glass. However, the relative density of these samples increases with increasing glass content to ~ 78 % for the samples containing 25 % glass as the different secondary phases form; even so, this density is over 15 % lower than for the pure HA phase at the same temperature, once again confirming that the reaction of HA with the glass results in formation of porosity.

3.5 HA–glass composites sintered at 1200 °C

The pure HA samples sintered at 1200 °C display degradation with some α-TCP phase forming. The α-TCP is also present as 5 wt% glass is incorporated and disappears with further increase in glass content. This is most likely due to the increased level of β-TCP that occurs with increasing glass content. The other phases present in the samples sintered at 1200 °C are present in very similar levels to those in the samples sintered at 1100 °C, with the exception of calcium oxide which is not present at 1200 °C.

The pure HA samples sintered at 1200 °C display the same relative density, Fig. 12, of ~ 94 %, as samples sintered at 1100 °C. The samples sintered at 1200 °C, as with those sintered at 1000 °C and 1100 °C, experience a decrease in density from 2.89 g/cm^3 for pure HA to 2.39 g/cm^3 for HA with 5 wt% glass. However, the decrease is not as substantial as for the samples sintered at 1100 °C. With

increasing glass content, the samples sintered at 1200 °C do not experience a linear increase in density. Only the samples containing 5 wt% and 15 wt% glass display a statistical difference of all the glass samples, while the other samples exhibit densities comparable to the pure HA (0 wt% glass). With 10 wt% addition of glass, the relative density of the samples sintered at 1200 °C increases to the same density exhibited by the pure HA samples. With further increases in glass content to 15 wt% the densities decrease again to a relative density of ~ 76 wt%. Increasing the glass content to 20 and 25 wt% results in increases in density to levels approximately the same as for the pure HA samples, i.e. 90 % and 94 %, respectively.

Figure 13 shows SEM images of the HA/glass composites sintered at 1200 °C for 2 h. The samples with 0, 5 and 10 wt% glass content, seen in Fig. 13a–c, are relatively

dense materials with fairly homogeneous surfaces. Figure 13d displays quite a different microstructure for HA containing 15 wt% glass with large areas where the liquid phase has coalesced interspersed with large pores. Figure 13e for the materials containing 20 % glass shows large areas of relatively small interconnected pores within which are areas of fully dense material formed from the liquid and remaining as glass phase. Figure 13f for the material containing 25 % glass clearly shows a number of different phases, as was evident from XRD, with dense regions surrounded by large areas of porosity.

3.6 Strength and Weibull

Figure 14 details the change in median biaxial flexural strength, herein referred to as simply BFS, for HA/glass
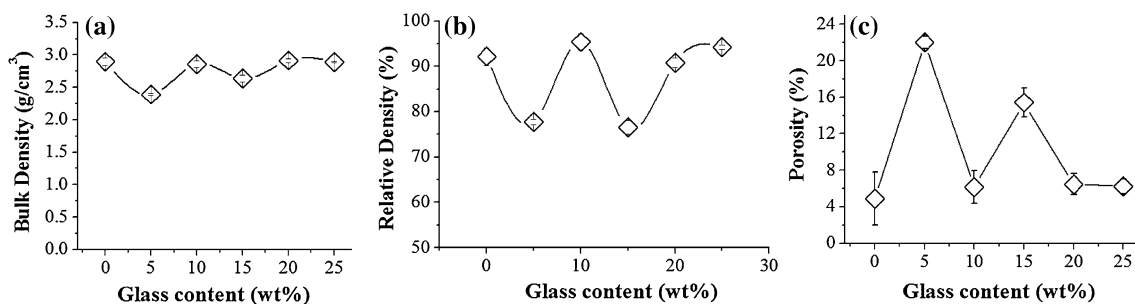

Fig. 12 **a** bulk density, **b** relative density **c** porosity of HA/glass composites sintered at 1200 °C for 2 h
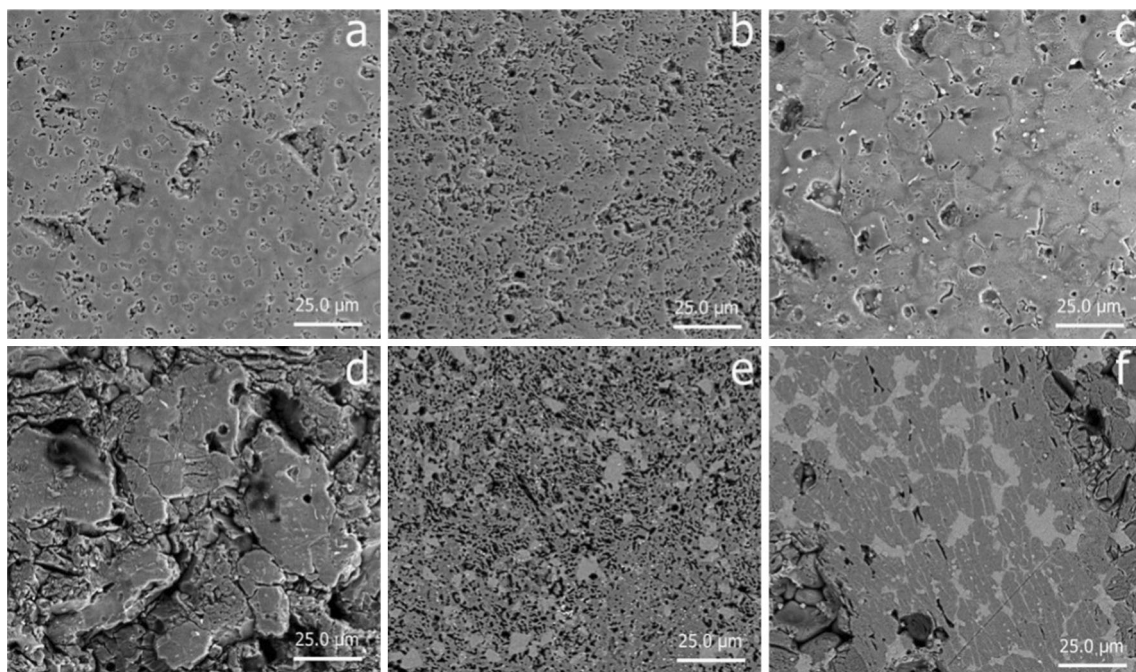

Fig. 13 SEM micrographs for HA/glass composites sintered at 1200 °C for 2 h: **a** pure HA, **b** HA/5 % glass, **c** HA/10 % glass, **d** HA/15 % glass, **e** HA/20 % glass and **f** HA/25 % glass
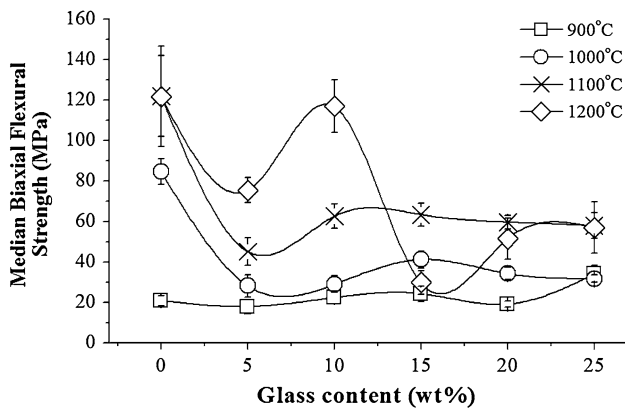
Fig. 14 The median biaxial flexural strength (BFS) with standard deviations of HA/glass composites sintered at four different temperatures for 2 h

Table 2 Weibull modulus of HA and HA/glass composites sintered at 900, 1000, 1100 and 1200 °C for 2 h

Glass content (%)	900 °C	1000 °C	1100 °C	1200 °C
0	10	18	7	5
5	5.5	8	8	14
10	11	20	12	10
15	5	11	13	5
20	18	13	22	6
25	11	21	11	4

composites with increasing glass content for each sintering temperature. The HA sintered at 900 °C exhibited a BFS of 21 MPa that increases by 13 MPa in conjunction with an increase in glass content up to 25 wt%. The composites sintered at 1000 °C experience a relatively linear decrease in strength with increasing glass content, from 84 MPa in the pure HA samples to 32 MPa in the samples containing 25 wt% glass. In much the same manner, the samples sintered at 1100 °C experience a decrease in strength with added glass content; the samples containing 5 wt% glass experience a decrease in strength of approximately 64 MPa compared to the pure HA samples. Strength increases to 63 MPa with 10 wt% glass, which remains statistically constant up to 25 wt% additions of glass. The samples sintered at 1200 °C experience a very similar trend to the samples containing 5, 10 and 15 wt% glass sintered at 1100 °C with the same glass contents, albeit with higher values. The strength of the samples of HA containing 5 wt% glass decreases to 75 MPa from 122 MPa for the pure HA. With 10 wt% glass, the strength, of 116 MPa, is very similar to that for the pure HA samples. The samples with 15 wt% glass experience a large decrease in strength compared to the samples with 10 wt% glass, with a decrease in BFS to 30 MPa. Upon increasing the glass content to 20 wt% and 25 wt%, the BFS increases to 51 MPa and 56 MPa, respectively.

Table 2 shows the Weibull modulus, a measure of reliability, for each of the HA/glass compositions at each sintering temperature. The modulus values at each sintering temperature do not show any trend across all wt% glass additions.

4 Discussion

From the results of this study, pure HA is stable up to 1100 °C with only a slight degradation to α-TCP at 1200 °C and relative densities of >90 % are achieved at 1100–1200 °C.

Differential thermal analysis (Fig. 2) shows the endothermic and exothermic reactions occurring up to the liquidus temperature. The resulting phases formed due to the various reactions were detailed using X-ray diffraction (Fig. 3). Upon raising the temperature to approximately 800 °C, the main phases crystallised from the glass were $Na_2Zn_3(SiO_4)$, $CaTiO_3$, $ZnSiO_3$ and ZnO and above 890 °C, melting occurs.

Upon addition of 5 wt% glass, which is liquid above 890 °C, the HA begins to degrade to form >40 % β-tricalcium phosphate (β-TCP). Santos et al. [44] show that sodium oxide (Na_2O) in the glass, which accounts for 17 % of the glass content in this study, results in increased destabilisation of the HA by removing the hydroxyl group, resulting in increased decomposition to TCP. Kangasniemi et al. [45] also reported this along with the formation of rhenanite ($CaNaPO_4$), which was not observed in this study irrespective of sintering temperature. Thus although the presence of Na_2O in the glass/liquid may be the cause of the HA destabilisation, the resultant crystalline phases do not include Na in any form. Knowles et al. [46] also noted a lack of crystalline phase formation with Na^+ when sintering HA reinforced with $Na_2O–P_2O_5$ glass. The fact that multi-pattern refinement confirms the lack of any Na containing crystalline phase implies that Na remains in the liquid phase and cools to form a residual glass, and this may be a factor affecting densification.

The formation of TCP however is not detrimental to the composite as TCP is a calcium deficient form of HA and, as such, resembles the calcium deficient structure of natural bone and displays bioactivity [47]. However TCP can exhibit instability above a pH of 4.2, which may lead to interaction with body fluid on its surfaces [48]. When this occurs in vivo, HA forms on the surface of the β-TCP implant and the pH of the local solution around the implant decreases [49] leading to increased solubility [48] that may be detrimental to the longevity of the implant. Conversely, this also offers the potential to design a therapeutic implant that reabsorbs in tandem with bone growth, releasing ions

into the surrounding tissue. In mechanical terms, TCP provides greater strengths [50], thus this formation may add to the overall strength of the composite.

With an increase in glass content to 10 wt%, HA decomposes further producing increased amounts of TCP. In addition, hardystonite ($Ca_2ZnSi_2O_7$), which has relatively high strength [51] and biocompatibility [52], also forms. These three crystalline phases exist up to the 25 wt% glass loading, with the main calcium phosphate phase now being β-TCP and hardystonite being present in nearly equal quantities to HA. Thus the reaction between the HA and glass/liquid at 900 °C has resulted in a glass–ceramic composite that contains bioactive phases. Due to the low sintering temperature these phase interactions have a negligible effect on the overall density of the samples (Fig. 8) and strength of the composites (Fig. 14). It should be noted that the glass phase is in liquid form at the sintering temperatures used in this study (>900 °C), and it would be expected that overall densification should increase due to liquid phase sintering, particularly as sintering temperature is increased.

A sintering temperature of 1000 °C results in increased decomposition of the HA and increased formation of the β-TCP as glass content increases, with HA ceasing to exist in any detectable amount in composites with >15 wt% glass additions. Hardystonite also forms at the same glass loading and in similar amounts to that in the composites sintered at 900 °C. The increased temperature also results in the formation of two calcium phosphate phases, monocalcium phosphate monohydrate ($Ca(H_2PO_4)_2 \cdot H_2O$), or MCPM, and calcium pyrophosphate dihydrate ($Ca_2P_2O_7 \cdot 2H_2O$), in the samples containing 15 and 20 wt% glass. It is probable that the presence of the glass phase is having an effect on the decompositional phase assemblage. Further research into the formation of these two decompositional phases is out of the remit of this paper, but may be investigated in future work.

However, MCPM is a decompositional product of HA and is the final phase of HA decomposition [53]. As such, the decomposition of HA to MCPM displays the level that decomposition that can take place. It is also a soluble calcium phosphate and, consequently, it is generally used as a precursor for precipitation of HA [54] in synthesis reactions. Calcium pyrophosphate dihydrate has been shown to aid sintering of TCP when added in small quantities of 0.5–3 wt% by stabilising the β-TCP phase, delaying the transformation to α-TCP which prevents further densification at temperatures ∼1200 °C [55]. Although the sintering temperature of 1000 °C is generally too low for the formation of α-TCP, this does not eliminate the possibility of β-TCP stabilisation taking place, although the relatively high levels of calcium pyrophosphate may have a negative effect on stabilisation; however this is unknown from this study. From a biological standpoint, pyrophosphate is thought to play a role in bone mineralisation [56] and as such a calcium pyrophosphate would be attractive as a bone replacement, although not many reports are available in the literature on this subject. Thus, although the HA phase is decomposing to other calcium phosphate phases and the level of reactions is increasing between the ceramic and glass/liquid phases due to the increased sintering temperature, the resultant composite still presents as a bioactive material. However the increase in strength compared to the 900 °C samples is relatively small, which can be attributed to the lack of densification.

Continuing to increase the sintering temperature to 1100 °C results in decomposition of the HA phase and the formation of β-TCP with increasing glass content in much the same way as at the lower sintering temperatures. However, the amount of β-TCP generated is less than that observed in the samples sintered at 1000 °C, implying that there may be a stabilising effect on the HA. At 15 wt% glass additions the samples sintered at 1100 °C form further phases with the generation of calcium phosphate based phases; namely dicalcium phosphate anhydrous—DCPA—($CaHPO_4$), which is also known as monetite, and calcium pyrophosphate dihydrate ($Ca_2P_2O_7 \cdot 2H_2O$), which also formed in the HA samples with 20 wt% glass that were sintered at 1000 °C. Monetite is used as a component in the apatite powders employed in self-hardening CaP pastes used for skeletal applications [57], as such this presents a bioactive aspect to its formation in these composites. The presence of calcium titanate ($CaTiO_3$) may have a positive effect on the stability of the calcium phosphate phases present in the samples as it is more stable in low pH environments than both HA and TCP [58]. In addition, the presence of $CaTiO_3$ increases osteoblast adhesion compared to both HA and Ti which may increase overall bioactivity [59]. For example, Manso et al. [59] show that significant apatite growth on $CaTiO_3$ does occur in SBF, accentuating the bioactive properties of this phase. Increasing the glass content results in the formation of dicalcium silicate (Ca_2SiO_4). This has been shown to be a promising implant material due to its good bioactivity, biocompatibility and mechanical properties [60, 61]. Willemite (Zn_2SiO_4) has been shown to have excellent biocompatibility [62, 63]. Thus the formation of these phases may add to the overall bioactivity of the material.

Further to increasing the phase assemblage of the composite, the increasing additions of glass above 5 wt% content also results in an increase in the strengths. However, overall the addition of the glass phase results in a decrease in strength when compared to the pure HA samples sintered at 1100 °C. The evidence so far implies that the addition of glass, irrespective of wt%, does not add to the densification process, which should be expected due to

liquid phase sintering provided by the glass/liquid phase. In fact, the presence of the glass phase seems to impede densification, resulting in samples with decreased density and strengths.

Increasing the sintering temperature to 1200 °C leads to the formation of a small amount of α-TCP in the pure HA composition and much more α-TCP for HA with 5 wt% glass with a small reduction in β-TCP. Above 5 wt% glass loadings the α-TCP disappears. This suggests that the α-TCP is unstable in the presence of the liquid phase at this temperature. It is interesting to note that the samples with 10 to 15 wt% addition of glass retain about the same level of HA as was observed in the samples sintered at 1000 and 1100 °C. This could be due to the stabilising nature of titanate on the calcium phosphate phases. Overall, the decomposition of HA and the phase assemblage development follows similar trends to the lower sintering temperatures. The HA/glass samples sintered at 1200 °C experience an increase in density compared to their 1100 °C counterparts, and the samples containing 10, 20 and 25 wt% glass experience densities comparable to the pure HA samples with 0 wt% glass. However, this does not equate to comparable strengths to the pure HA samples sintered at 1200 °C. In fact, the samples with glass content greater than 10 wt% experience a decrease in strength below that of their 1100 °C counterparts, irrespective of the increased density. Thus, the addition of glass appears to inhibit the densification process of the HA/glass composites, which is most evident in the HA samples with 5 wt% additions of glass.

Liquid phase sintering is occurring in these samples, as the glass melting temperature is below 900 °C (Fig. 2), and it has been shown in other studies that 5 % of the amount of the solid matrix phase should be sufficient to allow liquid phase sintering to occur [64–66]. Santos et al. [65] use 2.5 wt% glass phase with varying number of oxides present, collectively P_2O_5, CaO, Na_2O, Al_2O_3, SiO_2, in a HA matrix and achieve densities in the range of ∼97 % at temperatures of 1200 and 1300 °C. Lopes et al. [66] also obtain increased densities and strengths with the introduction of a glass phase (varying amounts of P_2O_5, CaO, CaF_2, MgO) in proportions of 2.5 and 4 wt% of the HA phase with temperatures above 1250 °C. A study by Oktar et al. [64] also showed that glass additions, with constituents of P_2O_5, CaO and Na_2O, up to 5 and 10 wt% of the HA phase, can increase the mechanical properties of HA compared to pure HA. Thus the 5 wt% glass loadings in this work would be expected to increase density, and possibly strength, compared to their HA counterparts.

One major difference between those reports in the literature and this study is the composition of the glass phase with the inclusion of Na_2O, as already discussed, and the absence of P_2O_5. Georgiou et al. [50] state that phosphate glasses when incorporated into HA, melt at a lower temperature compared to HA and can act to increase density by enhancing the sintering mechanisms which greatly enhances mechanical properties. This is said to occur as the liquid phosphate phase acts on the solid HA particles to reduce interfacial energy and promote the kinetics of the sintering process by a faster diffusion than the concurrent solid state process of single HA [44]. Oktar et al. [64] show that the oxide content was also a determining factor with HA/10 wt% three-constituent oxide (P_2O_5, CaO, Na_2O) samples exhibiting decreased density and strength compared with the HA/10 wt% two-constituent oxide (P_2O_5, CaO) samples at the same temperature. Thus the choice of glass composition may be a factor in the lack of densification of all the samples with 5 wt% glass content, and higher. One important similarity between these studies that display increased densities and strength, is the use of a phosphate based phase in the glass. Thus, glass composition is a crucial variable in allowing liquid phase sintering of HA to occur without decomposition and leading to densification.

5 Conclusions

This paper investigated the use of a glass phase (CaO–TiO_2–Na_2O–ZnO–SiO_2) in an attempt to allow phase interaction with a HA matrix, to form bioactive phases with a parallel increase in strength of the composite. The following points were concluded from this research.

- Both increasing temperature and increasing glass loadings result in HA decomposition.
- Bioactive phases can be formed due to the interactions of the HA and glass phase.
- Although sodium (Na_2O) is in the glass phase, no Na_2O containing phase occurs in the final phase assemblages indicating the possibility of the formation of an Na_2O residual glass.
- The addition of 5 % glass does not result in increased densification even though the glass is in a liquidus phase and liquid phase sintering (LPS) is occurring. Increasing the glass content results in an increase in density, however this is still below the density of the original pure HA for the 900, 1000 and 1100 °C samples. Only the 1200 °C HA–glass samples attain similar densities.
- Overall samples strength decreases with 5 % glass additions across all temperatures above 900 °C. Increasing the sintering temperature and increasing glass additions results in strength fluctuation that show no trends.
- No increased reliability was achieved with incremental glass additions.

It is highly likely that the inclusion of Na_2O and the absence of P_2O_5 in the starting glass resulted in the interactions between the HA and glass phase that resulted in the reduced densification and lack of strength. These results are counter to other studies that did experience an increase in the properties when using a phosphate based glass.

References

1. Kalita S, Bhardwaj A, Bhatt H. Nanocrystalline calcium phosphate ceramics in biomedical engineering. Mater Sci Eng C. 2007;27(3):441–9.

2. Wang M. Developing bioactive composite materials for tissue replacement. Biomaterials. 2003;24(13):2133–51.

3. Manley M, Sutton K, Dumbleton J. Calcium phosphates: a survey of the orthopaedic literature. In: Epinette J, Manley M, editors. Fifteen years of clinical experience with hydroxyapatite coatings in joint arthroplasty. 452 New York: Springer; 2003. p. 452.

4. Itoh S, Kikuchi M, Takakuda K, Koyama Y, Matsumoto H, Ichinose S, et al. The biocompatibility and osteoconductive activity of a novel hydroxyapatite/collagen composite biomaterial, and its function as a carrier of rhBMP-2. J Biomed Mater Res. 2001;54(3):445–53.

5. Anselme K, Noël B, Flautre B, Blary M, Delecourt C, Descamps M, et al. Association of porous hydroxyapatite and bone marrow cells for bone regeneration. Bone. 1999;25(2, Supplement 1):51S–54S.

6. Erbe E, Marx J, Clineff T, Bellincampi L. Potential of an ultra-porous β-tricalcium phosphate synthetic cancellous bone void filler and bone marrow aspirate composite graft. Eur Spine J. 2001;10(2):S141–6.

7. Klein C, Driessen A, de Groot K, van den Hooff A. Biodegradation behavior of various calcium phosphate materials in bone tissue. J Biomed Mater Res. 1983;17(5):769–84.

8. Hayek E, Newesely H, Rumpel M. Pentacalcium Monohydroxyorthophosphate. In: Kleinberg J, editor. Inorganic Syntheses [Internet]. New York: Wiley; 2007. p. 63–5. http://onlinelibrary.wiley.com/doi/10.1002/9780470132388.ch17/summary. Accessed 9 Jun 2013.

9. Royer A, Viguie J, Heughebaert M, Heughebaert J. Stoichiometry of hydroxyapatite: influence on the flexural strength. J Mater Sci Mater Med. 1993;4(1):76–82.

10. Ramachandra Rao R. Synthesis and sintering of hydroxyapatite–zirconia composites. Mater Sci Eng C. 2002;20(1–2):187–93.

11. Ioku K, Yoshimura M, Sōmiya S. Microstructure and mechanical properties of hydroxyapatite ceramics with zirconia dispersion prepared by post-sintering. Biomaterials. 1990;11(1):57–61.

12. Guo H. Laminated and functionally graded hydroxyapatite/yttria stabilized tetragonal zirconia composites fabricated by spark plasma sintering. Biomaterials. 2003;24(4):667–75.

13. Sung Y, Shin Y, Ryu J. Preparation of hydroxyapatite/zirconia bioceramic nanocomposites for orthopaedic and dental prosthesis applications. Nanotechnology. 2007;18(6):065602.

14. Yoshida K. Fabrication of structure-controlled hydroxyapatite/zirconia composite. J Eur Ceram Soc. 2006;26(4–5):515–8.

15. Rao W, Boehm R. A study of sintered apatites. J Dent Res. 1974;53(6):1351–4.

16. Jarcho M, Bolen C, Thomas M, Bobick J, Kay J, Adamson R. Hydroxylapatite synthesis and characterization in dense polycrystalline form. J Mater Sci. 1976;11(11):2027–35.

17. Nagarajan V, Rao K. Structural, mechanical and biocompatibility studies of hydroxyapatite-derived composites toughened by zirconia addition. J Mater Chem. 1993;3(1):43–51.

18. Hing K, Gibson I, Di-Silvio L, Best S, Bonfield W. Effect of variation in Ca: P ratio on cellular response of primary human osteoblast-like cells to hydroxyapatite-based ceramics. Bioceramics Conference. 1998. p. 293–6.

19. Curran D, Fleming T, Towler M, Hampshire S. Mechanical properties of hydroxyapatite–zirconia compacts sintered by two different sintering methods. J Mater Sci Mater Med. 2010;21(4):1109–20.

20. Adolfsson E, Alberius-Henning P, Hermansson L. Phase analysis and thermal stability of hot isostatically pressed zirconia–hydroxyapatite composites. J Am Ceram Soc. 2000;83(11):2798–802.

21. Li J, Hermansson L, Söremark R. High-strength biofunctional zirconia: mechanical properties and static fatigue behaviour of zirconia–apatite composites. J Mater Sci Mater Med. 1993;4(1):50–4.

22. Shen Z, Adolfsson E, Nygren M, Gao L, Kawaoka H, Niihara K. Dense hydroxyapatite–zirconia ceramic composites with high strength for biological applications. Adv Mater. 2001;13(3):214–6.

23. Li W. Fabrication of HAp–ZrO2 (3Y) nano-composite by SPS. Biomaterials. 2003;24(6):937–40.

24. Choi J, Kong Y, Kim H, Lee I. Reinforcement of hydroxyapatite bioceramic by addition of Ni_3Al and Al_2O_3. J Am Ceram Soc. 1998;81(7):1743–8.

25. Asmus S, Sakakura S, Pezzotti G. Hydroxyapatite toughened by silver inclusions. J Compos Mater. 2003;37(23):2117–29.

26. Chaki T, Wang P. Densification and strengthening of silver-reinforced hydroxyapatite-matrix composite prepared by sintering. J Mater Sci Mater Med. 1994;5(8):533–42.

27. Zhang X, Gubbels G, Terpstra R, Metselaar R. Toughening of calcium hydroxyapatite with silver particles. J Mater Sci. 1997;32(1):235–43.

28. Nath S, Kalmodia S, Basu B. Densification, phase stability and in vitro biocompatibility property of hydroxyapatite-10 wt% silver composites. J Mater Sci Mater Med. 2010;21(4):1273–87.

29. Kokubo T, Shigematsu M, Nagashima Y, Tashiro M, Nakamura T, Yamamuro T, et al. Apatite-and wollastonite-containing glass-ceramics for prosthetic application. Bull Inst Chem Res Kyoto Univ. 1982;60(3–4):260–8.

30. Wren A, Boyd D, Towler MR. The processing, mechanical properties and bioactivity of strontium based glass polyalkenoate cements. J Mater Sci Mater Med. 2008;19(4):1737–43.

31. Williams J, Billington R. Changes in compressive strength of glass ionomer restorative materials with respect to time periods of 24 h to 4 months. J Oral Rehabil. 1991;18(2):163–8.

32. Ruys A, Wei M, Sorrell C, Dickson M, Brandwood A, Milthorpe B. Sintering effects on the strength of hydroxyapatite. Biomaterials. 1995;16(5):409–15.

33. Liu D, Chou H. Formation of a new bioactive glass-ceramic. J Mater Sci Mater Med. 1994;5(1):7–10.

34. Kokubo T. Bioactive glass ceramics: properties and applications. Biomaterials. 1991;12(2):155–63.

35. Ravaglioli A, Krajewski A, De Portu G. Problems involved in assessing mechanical behaviour of bioceramics. Bioceramics. 1989;18:13–8.

36. Xiang Y, Du J, Skinner L, Benmore C, Wren A, Boyd D, et al. Structure and diffusion of ZnO–SrO–CaO–Na_2O–SiO_2 bioactive glasses: a combined high energy X-ray diffraction and molecular dynamics simulations study. RSC Adv. 2013;3(17):5966.

37. Wren AW, Keenan T, Coughlan A, Laffir FR, Boyd D, Towler MR, et al. Characterisation of Ga_2O_3–Na_2O–CaO–ZnO–SiO_2 bioactive glasses. J Mater Sci. 2013;48(11):3999–4007.

38. Wren A, Coughlan A, Smale K, Misture S, Mahon B, Clarkin O, et al. Fabrication of CaO–NaO–SiO_2/TiO_2 scaffolds for surgical applications. J Mater Sci Mater Med. 2012;23(12):2881–91.

39. Wren A, Akgun B, Adams B, Coughlan A, Mellott N, Towler M. Characterization and antibacterial efficacy of silver-coated Ca–Na–Zn–Si/Ti glasses. J Biomater Appl. 2012;27(4):433–43.

40. Brook I, Freeman C, Grubb S, Cummins N, Curran D, Reidy C, et al. Biological evaluation of nano-hydroxyapatite–zirconia (HA–ZrO2) composites and strontium–hydroxyapatite (Sr–HA) for load-bearing applications. J Biomater Appl. 2012;27(3):291–8.

41. Towler M, Hampshire S, Reidy D, Curran D, Fleming T. Comparison of microwave and conventionally sintered yttria doped zirconia ceramics and hydroxyapatite-zirconia nanocomposites. In: Ohji T, Singh M, editors. Advanced Processing and Manufacturing Technologies for Structural and Multifunctional Materials V: Ceramic Engineering and Science Proceedings. New York: Wiley; 2011.

42. Williams J, Billington R, Pearson G. The effect of the disc support system on biaxial tensile strength of a glass ionomer cement. Dent Mater. 2002;18(5):376–9.

43. Quinn J, Quinn G. A practical and systematic review of Weibull statistics for reporting strengths of dental materials. Dent Mater. 2010;26(2):135–47.

44. Santos J, Knowles J, Reis R, Monteiro F, Hastings G. Microstructural characterization of glass-reinforced hydroxyapatite composites. Biomaterials. 1994;15(1):5–10.

45. Kangasniemi I, DeGroot K, Wolke J, Andersson O, Luklinska Z, Becht J, et al. The stability of hydroxyapatite in an optimized bioactive glass matrix at sintering temperatures. J Mater Sci Mater Med. 1991;2(3):133–7.

46. Knowles J, Bonfield W. Development of a glass reinforced hydroxyapatite with enhanced mechanical properties. The effect of glass composition on mechanical properties and its relationship to phase changes. J Biomed Mater Res. 1993;27(12):1591–8.

47. Kondo N, Ogose A, Tokunaga K, Umezu H, Arai K, Kudo N, et al. Osteoinduction with highly purified β-tricalcium phosphate in dog dorsal muscles and the proliferation of osteoclasts before heterotopic bone formation. Biomaterials. 2006;27(25):4419–27.

48. Cao W, Hench L. Bioactive materials. Ceram Int. 1996;22(6):493–507.

49. Hench L. Bioceramics: from concept to clinic. J Am Ceram Soc. 1991;74(7):1487–510.

50. Georgiou G, Knowles J. Glass reinforced hydroxyapatite for hard tissue surgery—Part 1: mechanical properties. Biomaterials. 2001;22(20):2811–5.

51. Wu C, Chang J, Zhai W. A novel hardystonite bioceramic: preparation and characteristics. Ceram Int. 2005;31(1):27–31.

52. Lu H, Kawazoe N, Tateishi T, Chen G, Jin X, Chang J. In vitro proliferation and osteogenic differentiation of human bone marrow-derived mesenchymal stem cells cultured with hardystonite (Ca2ZnSi2O7) and β-TCP ceramics. J Biomater Appl. 2010;25(1):39–56.

53. Bohner M. Calcium orthophosphates in medicine: from ceramics to calcium phosphate cements. Injury. 2000;31(Supplement 4):D37–47.

54. Jinawath S, Pongkao D, Suchanek W, Yoshimura M. Hydrothermal synthesis of monetite and hydroxyapatite from monocalcium phosphate monohydrate. Int J Inorg Mater. 2001;3(7):997–1001.

55. Ryu H, Youn H, Sun Hong K, Chang B, Lee C, Chung S. An improvement in sintering property of β-tricalcium phosphate by addition of calcium pyrophosphate. Biomaterials. 2002;23(3):909–14.

56. Hessle L, Johnson K, Anderson H, Narisawa S, Sali A, Goding J, et al. Tissue-nonspecific alkaline phosphatase and plasma cell membrane glycoprotein-1 are central antagonistic regulators of bone mineralization. Proc Natl Acad Sci. 2002;99(14):9445–9.

57. Ooms E, Wolke J, van de Heuvel M, Jeschke B, Jansen J. Histological evaluation of the bone response to calcium phosphate cement implanted in cortical bone. Biomaterials. 2003;24(6):989–1000.

58. Asami K, Saito K, Ohtsu N, Nagata S, Hanawa T. Titanium-implanted CaTiO3 films and their changes in Hanks' solution. Surf Interface Anal. 2003;35(5):483–8.

59. Manso M, Langlet M, Martinez-Duart J. Testing sol–gel CaTiO3 coatings for biocompatible applications. Mater Sci Eng C. 2003;23(3):447–50.

60. Gou Z, Chang J, Zhai W. Preparation and characterization of novel bioactive dicalcium silicate ceramics. J Eur Ceram Soc. 2005;25(9):1507–14.

61. Liu X, Xie Y, Ding C, Chu P. Early apatite deposition and osteoblast growth on plasma-sprayed dicalcium silicate coating. J Biomed Mater Res A. 2005;74A(3):356–65.

62. Zhang M, Zhai W, Chang J. Preparation and characterization of a novel willemite bioceramic. J Mater Sci Mater Med. 2010;21(4):1169–73.

63. De Aza P, Guitian F, De Aza S. Bioactivity of wollastonite ceramics: in vitro evaluation. Scr Metall Mater. 1994;31(8):1001–5.

64. Oktar F, Göller G. Sintering effects on mechanical properties of glass-reinforced hydroxyapatite composites. Ceram Int. 2002;28(6):617–21.

65. Santos J, Reis R, Monteiro F, Knowles J, Hastings G. Liquid phase sintering of hydroxyapatite by phosphate and silicate glass additions: structure and properties of the composites. J Mater Sci Mater Med. 1995;6(6):348–52.

66. Lopes M, Monteiro F, Santos J. Glass-reinforced hydroxyapatite composites: fracture toughness and hardness dependence on microstructural characteristics. Biomaterials. 1999;20(21):2085–90.